Calibration of Dynamic Molecular Rulers Based on Plasmon Coupling between Gold Nanoparticles

Björn M. Reinhard,[†,‡] Merek Siu,[§] Harish Agarwal,[†] A. Paul Alivisatos,[∥,⊥] and Jan Liphardt*[,†,‡,§]

Physics Department, Biophysics Graduate Program, and Chemistry Department, University of California, Berkeley, California 94720, and Physical Biosciences Division and Materials Sciences Division, Lawrence Berkeley National Laboratory, Berkeley, California 94720

ABSTRACT

Pairs of noble metal nanoparticles can be used to measure distances via the distance dependence of their plasmon coupling. These "plasmon rulers" offer exceptional photostability and brightness; however, the advantages and limitations of this approach remain to be explored. Here we report detailed plasmon peak versus separation calibration curves for 42- and 87-nm-diameter particle pairs, determine their measurement errors, and describe experimental procedures to improve their performance in biology, nanotechnology, and materials sciences.

The characterization of nanometer-sized machines, such as artificial[1] and biological motors,[2] and of transient interactions between individual macromolecules requires stable and precise tools to measure absolute distances and distance changes. However, continuous monitoring of distances is challenging because of the small size of the systems of interest (tens of nanometers) and the extremely broad range of time scales. In cell differentiation and tissue growth, for example, relevant time scales range from nanoseconds to hours or longer. Molecular rulers based on single dye pair fluorescence resonance energy transfer (FRET)[3] have been the tool of choice for single-molecule measurements of distance changes.[4−7] However, like all fluorescence-based methods, FRET is constrained by the properties of organic dyes: a short lifetime (<180 s) when continuously illuminated and blinking due to trapping in dark states.[8,9] Conventional FRET measurements are also limited to a distance range of <10 nm,[10] complicating the investigation of the structural dynamics of large multicomponent systems such as the ribosome, the DNA loops formed during transcriptional regulation by distant enhancers,[11] and the folding/unfolding of large proteins or RNAs.

In cases where probes with a diameter of 30−40 nm can be tolerated, the limitations of FRET can be overcome with a dynamic molecular ruler based on the distance-dependent plasmon coupling of two noble metal nanoparticles.[12] A particle plasmon refers to the collective oscillation of the free electrons within a metal nanoparticle.[13] Noble metal nanoparticles are efficient light scatterers at their plasmon resonance frequency. The plasmon resonance frequency depends on the size[14−17] and shape of the particles,[15−19] the dielectric constant of the metal,[13,17,20] and the surrounding medium.[16,20−23] When two nanoparticles are brought into proximity (within ∼2.5 times the particle diameter)[24] their plasmons couple in a distance-dependent manner.[25] As the interparticle distance decreases, the coupled plasmon resonance wavelength red-shifts. The distance dependence of the plasmon coupling has been investigated at fixed interparticle distances with different nanostructures such as spherical,[26] cylindrical,[27,28] and elliptical nanoparticles,[29] trigonal prisms,[28] and opposing tip-to-tip Au triangle (bowtie) nanostructures.[30] In these studies, nanostructures were fabricated with top-down fabrication techniques such as electron beam lithography and thus had fixed interparticle spacing.

In contrast to the wealth of distance versus plasmon coupling data available for fixed geometries in optically homogeneous environments, there is currently very little information available for dynamic geometries in optically anisotropic environments. For the plasmon ruler to be a versatile and robust tool in biology and materials science, it is essential to obtain a wavelength versus distance relationship that is valid under typical experimental conditions: illumination by unpolarized light of functionalized particle dimers randomly oriented in space. Ruler calibration can be done experimentally (by measuring the resonance wavelength

* Corresponding author. E-mail: liphardt@physics.berkeley.edu.
† Physics Department, University of California, Berkeley.
‡ Physical Biosciences Division, Lawrence Berkeley National Laboratory.
§ Biophysics Graduate Program, University of California, Berkeley.
∥ Chemistry Department, University of California, Berkeley.
⊥ Materials Sciences Division, Lawrence Berkeley National Laboratory.
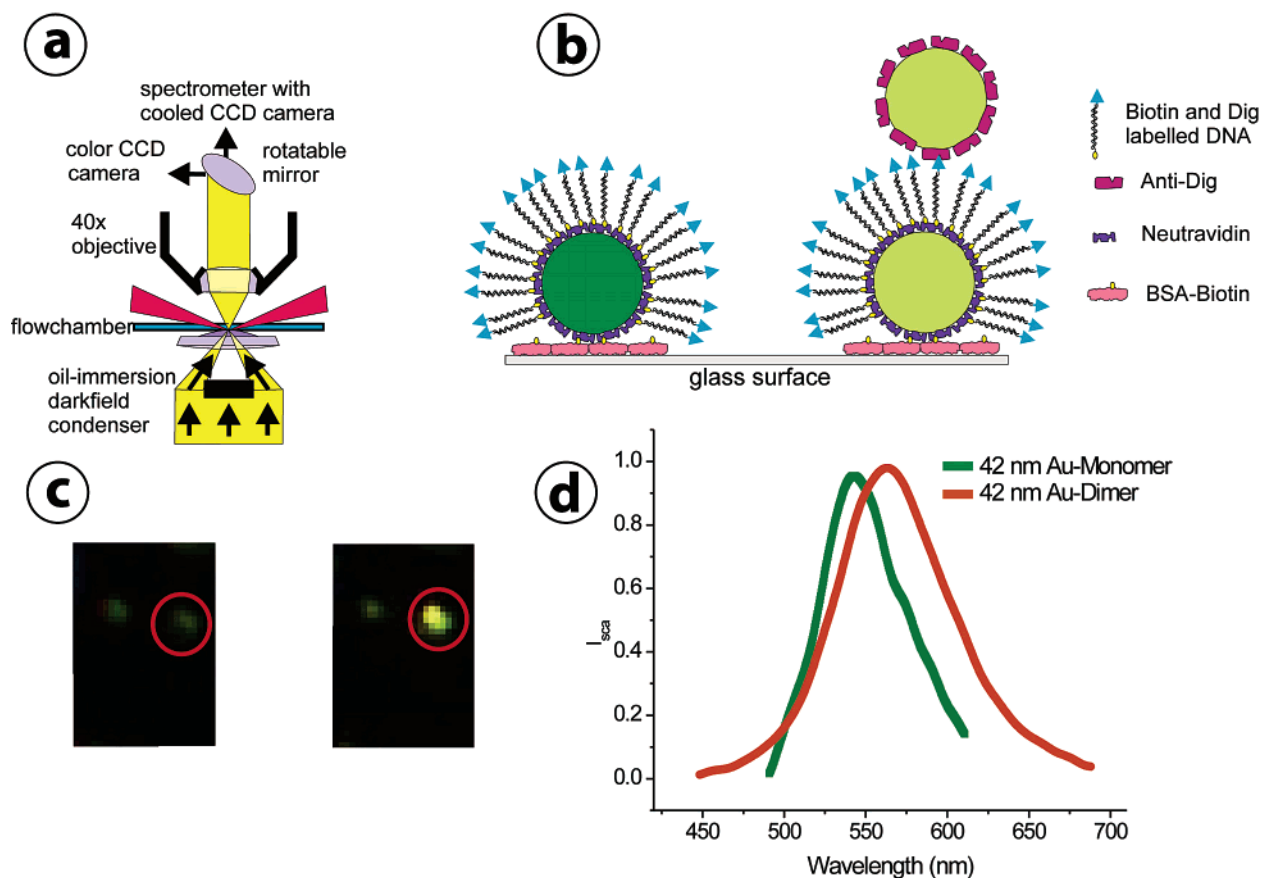
Figure 1. Darkfield microscopy of metal nanoparticles. (a) Experimental darkfield setup used for nanoparticle spectroscopy. (b) Directed assembly of plasmon rulers. First, a Neutravidin-coated nanoparticle is immobilized on a BSA-biotin functionalized surface. Then, a second antidigoxigenin coated nanoparticle is tethered to the immobilized nanoparticle using dsDNA that is labeled with both biotin and digoxigenin. (c) Dimer formation leads to a vivid change in color and intensity, which allows detection of assembled plasmon rulers "by eye". (d) Spectra before and after dimer formation for 42-nm gold particles (DNA tether length: 67 bps).

for a range of interparticle spacings) or theoretically, by solving Maxwell's equations. Here, we present a detailed experimental and theoretical study of the distance dependence of the plasmon resonance of single pairs of tethered gold (Au) nanoparticles with an average diameter of either 42 or 87 nm.

Plasmon Resonance versus Distance Relationship. We assembled dimers with various interparticle spacings and measured their plasmon resonance wavelength in a darkfield microscope using unpolarized white light (Figure 1a). We used dsDNA spacers of 10 (42-nm particles only), 20, 40, 67, 110, and 250 basepairs (bps) modified with biotin and digoxigenin at opposing ends to assemble dimers of anti-digoxigenin and surface-immobilized Neutravidin-coated gold nanoparticles (Figure 1b). Plasmon rulers are sensitive analytical tools, and their plasmon wavelength also depends on the ionic strength of the solution. To eliminate this influence, we recorded all of the spectra under identical buffer conditions (10 mM Tris, pH 7, 50 mM NaCl). For details concerning the synthesis of protein-coated nanoparticles and the directed assembly of plasmon rulers, please refer to the Supporting Information.

Double-stranded DNA was chosen as a spacer material because of its stiffness and well-understood synthesis and functionalization technologies. The interparticle separation,

x, is given by the sum of the end-to-end distance of the DNA and the thickness of the protein layer used to couple the DNA to the particles. The end-to-end distance of the DNA was obtained from its contour length using the wormlike-chain model[31] (using a persistence length of 53 nm[32] and a contour length per basepair of 0.34 nm), and the thickness of the protein layer was measured by dynamic light scattering to be ∼4 nm. Therefore, we added 8 nm to the DNA end-to-end distances to obtain the interparticle spacing.

We used a very weak criterion for dimer formation: any scattering source that changed intensity (Figure 1c) and color (Figure 1d) upon addition of complementary particles (typically ∼6% of all particles) was considered to be a dimer. Consequently, the results presented here represent a worst-case lower bound on the performance of contemporary plasmon rulers. Simple experimental procedures (described later) improve the accuracy and reliability of plasmon rulers substantially.

As can be seen in Figure 2a and b, the plasmon resonance distributions blue-shift with increasing interparticle distance. The distributions for the 87-nm plasmon rulers are consistently broader than those for the 42-nm particles. The average plasmon resonance peak wavelength, λ_{PR}, as a function of x is plotted in Figure 2c. We included data points for salt-precipitated 42- and 87-nm dimers at $x = 0$ and monomers
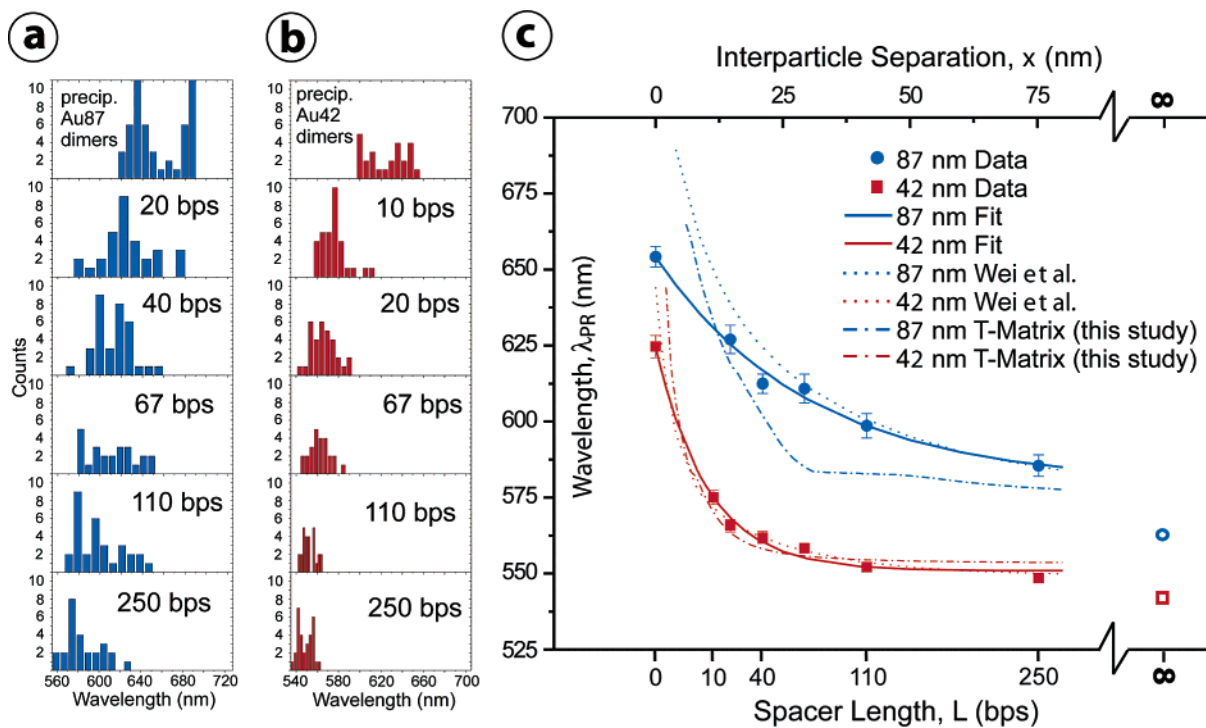
Figure 2. Plasmon resonance vs interparticle separation. Distributions of measured plasmon resonance wavelengths for selected dsDNA spacer lengths for (a) 87-nm Au plasmon rulers and (b) 42-nm Au plasmon rulers. We included data points for salt-precipitated dimers at $x = 0$. (c) Plot of the average plasmon resonance as a function of spacer length, L, (bottom axis) and approximated interparticle distance x (top axis) for 42- (red squares) and 87-nm (blue circles) plasmon rulers. The plasmon resonance wavelengths for dimers with infinite separations (=monomers) are included as open symbols. The reported errors are the standard errors of the mean. The continuous lines show fits (single exponentials $y(x) = A_0*\exp(-x/D_0) + C$) to the experimental data. Best-fit parameters for 42-nm Au particles: $C = 550.87$ nm, $A_0 = 73.48$ nm, $D_0 = 10.24$ nm; for 87-nm Au particles: $C = 579.66$ nm, $A_0 = 74.42$ nm, $D_0 = 30.23$ nm. The dotted lines represent T-matrix simulations by Wei et al.[29] assuming illumination with light polarized along the interparticle axis and dot−dashed lines are T-matrix simulations assuming nonpolarized illumination.

(corresponding to infinite separation) at $x = \infty$ nm. Our directed dimer assembly strategy requires dsDNA spacers and can therefore not generate dimers with zero separation. Instead we used salt-precipitated "dimers", which carry neither proteins nor dsDNA spacers. The salt-induced precipitation of bare Au nanoparticles cannot be well controlled. Indeed, there seem to be two separated populations of resonance wavelengths for salt-precipitated 87-nm Au nanoparticles, one centered at 635 nm and the other at 685 nm, indicating substantial contributions from larger agglomerates.

The measured resonance wavelength versus distance relationships are well-fit by simple exponentials (Figure 2c, continuous lines). Two qualitative trends are apparent. First, the peak resonance of the 87-nm dimers for all spacer lengths is consistently further in the red than for the 42-nm dimers. For particles with a diameter greater than 10 nm, the resonant peak energy (and therefore the peak wavelength) is expected to red-shift with increasing size because of electromagnetic retardation.[13] Second, the peak wavelengths blue-shift with increasing interparticle separation because of reduced near-field coupling, confirming and illustrating the physical principle underlying plasmon rulers.

The slopes of the $\lambda_{PR}(x)$ calibration curves bracket the useful dynamic range of the two rulers. The calibration curve for the 42-nm dimers has a steeper initial slope. Between $x = 0$ and $x = 14.7$ nm, the average peak wavelength has

already dropped by 58.9 nm. This drop is about 70% of the total spectral shift $\Delta\lambda_{PR}$ between dimers at $x = 0$ and monomers, which resemble noninteracting dimers at infinite separation. For the 87-nm particles, the average peak wavelength drops by 27.2 nm between $x = 0$ and $x = 14.7$ nm, which represents only about 30% of the total spectral change, $\Delta\lambda_{PR}$. For the largest spacer molecules ($x = 75.3$ nm) the measured plasmon wavelengths are still red-shifted with respect to the isolated monomers for both rulers. This indicates that there is still nonnegligible plasmon coupling between the gold particles at these distances. The spectral gap between monomers and dimers at 75.3 nm is distinctly smaller for 42-nm dimers ($\Delta\lambda_{PR} = 7.8$ nm) than for 87-nm dimers ($\Delta\lambda_{PR} = 22.7$ nm). Because of the steep slope of the $\lambda_{PR}(x)$ curve at short distances, the 42-nm plasmon ruler can best detect distance changes at short interparticle distances (<15 nm). For spacer lengths >20 bps, the slope in the λ_{PR}-(x) calibration curve is steeper for the 87-nm plasmon ruler, whereas the 42-nm curve has nearly converged. The 87-nm plasmon ruler thus covers a larger distance range, albeit with a reduced resolution.

One feature that is absent from our calibration curves deserves comment. Fromm et al.[30] demonstrated that for nanoparticle bowtie structures illuminated with light polarized along the interparticle axis the resonance shift changes sign at a critical interparticle distance. In our experiments, red-shifts with increasing x are not observed, indicating that the
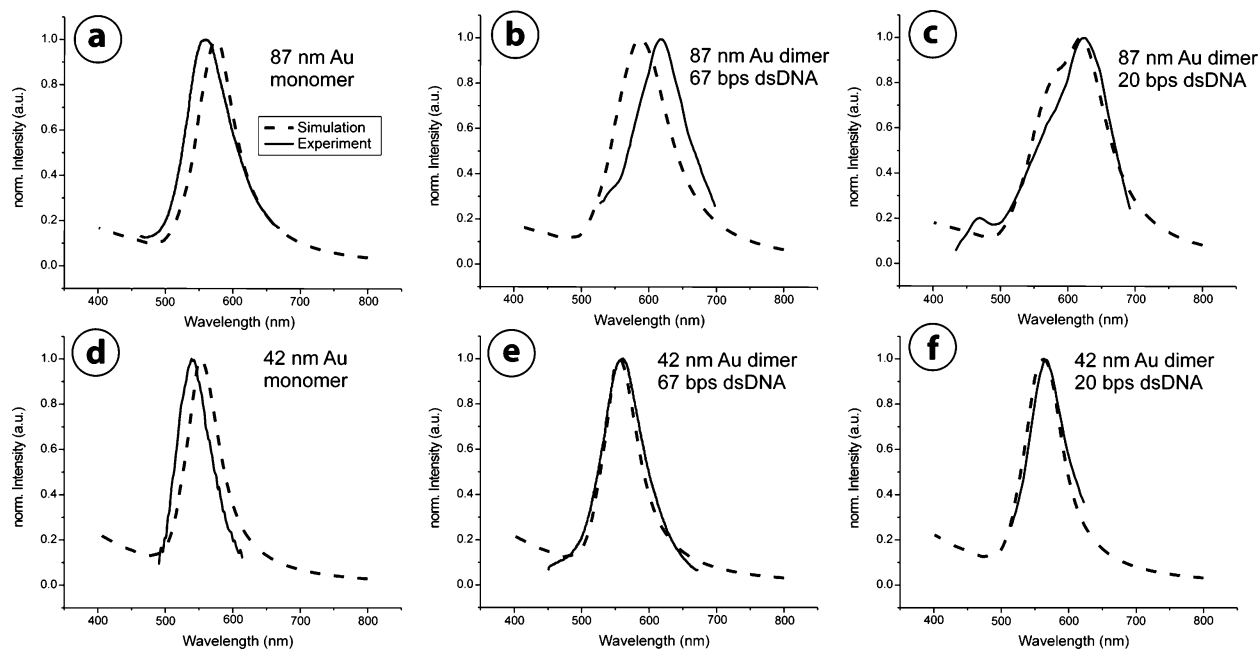
Figure 3. Comparison of measured and simulated spectra. Experimental and T-matrix simulated spectra (dashed line) for 87-nm Au dimers with (a) infinite separation, (b) 67 bps dsDNA spacer (29.3 nm), (c) 20 bps dsDNA spacer (14.7 nm), and for 42-nm Au dimers with (d) infinite separation, (e) 67 bps dsDNA spacer (29.3 nm), and (f) 20 bps dsDNA spacer (14.7 nm). For the simulations, illumination with unpolarized light was assumed.

investigated distance range is below the threshold at which the sign of the coupling reverses for spherical particles.

Simulations of Plasmon Shift versus Interparticle Spacing. Are our measurements consistent with theory and previous results? Recently, Wei et al.[29] obtained the wavelength versus distance relationships for pairs of bare 40- or 80-nm gold nanoparticles. In their simulations, they assumed that n_E (the refractive index of the particle's environment) was 1.5 and that the electromagnetic field was linearly polarized along a fixed interparticle axis. However, in potential biophysical or cell biological applications of plasmon rulers, the orientation of the interparticle axis relative to the incident light will typically vary with time. To approximate our experimental illumination conditions (the particles' random orientation in space and the use of unpolarized light), we simulated the plasmon shift versus interparticle separation relationship by averaging over a wide range of incident wave vectors and light polarizations (see the Supporting Information). In these calculations, we applied the discrete dipole approximation (DDA)[33] and the T-matrix method.[34] Although the actual experimental geometry is clearly more complex, we initially approximated the plasmon rulers by two spherical particles immersed in a homogeneous solution. This approximation was later relaxed. Figure 3 shows normalized spectra from typical experiments and our T-matrix simulations for 42- and 87-nm Au plasmon rulers at selected spacer lengths. The correspondence between experiment and simulation is very good for the peak width and shape; for the peak wavelength, correspondence is reasonable. Differences between experimental and calculated spectra can be due to the nonspherical shape of the real probes, formation of multiple tethers between the nanoparticles, as well as simplifications inherent in the T-matrix

simulations. Our calculations also do not account for protein functionalization of the nanoparticles, the ionic strength of the buffer, and the blocking reagent applied to the coverslip surface.

To partially account for these features of our experiments, we performed additional simulations in which n_E was a free parameter representing a weighted average of the various materials that surround the particle. The DDA approach reproduced the overall trend of the experimental data but because of the high computational cost of this method, we were unable to produce good fits to the data. We obtained the best agreement between the simulated and experimental data using a T-matrix calculation with $n_E = 1.6$. This refractive index is reasonable for protein-coated gold nanoparticles. Proteins typically have a refractive index of about 1.6, even when adsorbed.[35,36] The resulting curves are included in Figure 2c as dot−dashed lines. We also included the λ_{PR} versus x relationship predicted by Wei et al., assuming light polarized strictly along the interparticle axis (dashed lines). For the 42-nm plasmon rulers, our T-matrix simulations and those by Wei et al. show good quantitative agreement with the experimental data, except for the precipitated dimers at $x = 0$.

For the 87-nm plasmon rulers, both types of calculations fail to describe the experimental results over the complete distance range. The Wei et al. curve reports the plasmon peak due to light polarized along the symmetry axis, and therefore, driving the parallel mode. However, in our measured spectra (collected with unpolarized illumination), the perpendicular mode is present and distorts the spectra (Figure 3b and c). The perpendicular mode is most prominent at short interparticle separations, where the Wei et al. simulations perform most poorly. Our T-matrix simulations
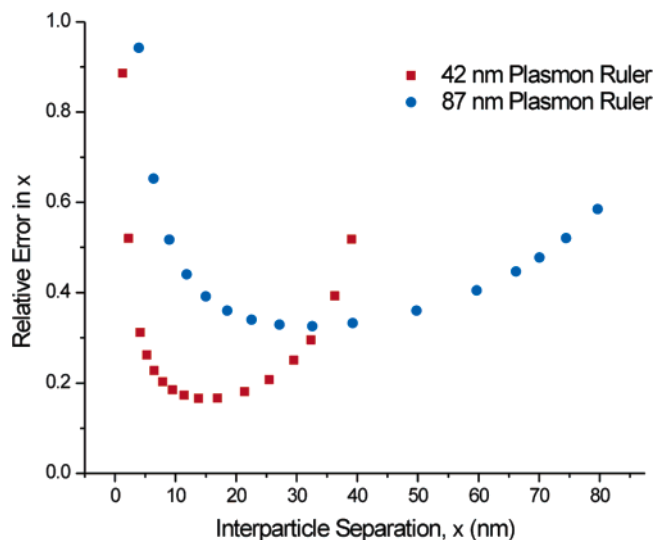
Figure 4. Distance dependence of the relative error, $\Delta x/x$, of two types of plasmon rulers. 42-nm Au plasmon rulers have the best spatial resolution at an interparticle separation of around 14 nm, 87-nm Au plasmon rulers exhibit highest resolution at 30 nm. The error curves intersect at $x = 32$ nm. At distances below this threshold, the 42-nm plasmon rulers are more precise than the 87-nm plasmon rulers.

do not fit the data at any separation, even though we averaged over many polarizations to account for the random orientation of the particles and the use of unpolarized light. The excellent fit of the Wei et al. curve to our data at larger separations suggests that our illumination light was partially polarized in the focal plane (along the ruler's symmetry axis) and the parallel mode thus dominates our signal. Given the geometry of darkfield illumination and the numerous reflecting surfaces between the light source and the sample, some degree of polarization cannot be excluded. In conclusion, the 42-nm rulers are much more robust toward polarization effects, and thus should be used in cases where the distance between particles is the primary desired readout. When larger particles are used to assemble plasmon rulers, polarization effects must be carefully accounted for. Of course, polarization sensitivity also has benefits because it can be used to determine the relative orientation of a plasmon ruler with respect to the polarization of the illumination light (via the relative height and position of the two plasmon peaks).

Measurement Errors. We quantified the magnitude and the distance dependence of the measurement error inherent to contemporary plasmon rulers. We fitted single exponentials to the upper and lower error bars of the $\lambda_{PR}(x)$ curves (Figure 2c) and inverted the resonance wavelength–distance relationship, yielding the measurement error, Δx, as a function of λ_{PR}. The absolute spatial resolution of plasmon rulers is distance dependent and decreases with increasing interparticle distance, and the relative error, $\Delta x/x$, is smallest around 15 nm (42-nm rulers) and 30 nm (87-nm rulers) (Figure 4). The larger rulers should be used in experiments where the typical separations are larger than the intersection of the two error curves in Figure 4 (32 nm). The measured spatial resolution is acceptable for many biophysical and cell

biological applications for separations <25 nm (42-nm rulers) or <65 nm (87-nm rulers).

What limits our ability to extract absolute distances from plasmon rulers? In principle, there should be no variation of the plasmon peak position for a given set of conditions. In practice, however, each particle dimer will differ from all other dimers, introducing measurement uncertainty. Numerous sources of dimer-to-dimer variations exist, including variation of the number of DNA tethers between the two particles and the precise diameter and shape of each particle.

The interparticle distance will decrease with increasing number of tethers. Under our experimental conditions, the number of dsDNA molecules bound to the functionalized nanoparticles is roughly 200 per 42-nm particle (Supporting Information Figure S1). This corresponds to an average surface coverage of 1 dsDNA molecule per $\sim$25 nm^2. Given this dsDNA density, the formation of multiple tethers between the nanoparticles cannot be excluded. Any variation of the number of tethers between the particles will broaden the distribution of the measured resonance wavelengths at a given spacer length. Because this error source is asymmetrical, that is, it can only *decrease* the interparticle spacing, the overall effect of multiple tethering will be to red-shift the average plasmon peak.

Particle heterogeneity is another major source of measurement uncertainty because the size and shape influence a particle's scattering spectrum and the surrounding field density. For example, triangular- and pentameric-shaped nanoparticles have different plasmon resonances than spherical particles.[14] Our commercially obtained "40"- and "80"-nm-diameter nanoparticle preparations had an actual diameter of 41.7 ± 3.1 nm and 86.9 ± 5.5 nm (Figure 5a and c), as judged from transmission electron microscopy (TEM) analysis of $\sim$125 particles per nominal diameter. Moreover, most particles are ellipsoidal with aspect ratios of $\sim$1.06 (Figure 5b and d); the TEM images also reveal that triangular and pentameric shapes occur in nonnegligible amounts (triangles: 3.3% (42 nm), 6.6% (87 nm); pentamers: 5.3% (42 nm), 4.8% (87 nm)) (Figure 5e). Thus, sphere−sphere dimers are likely to constitute $\sim$80% of all dimers, and sphere−triangle and sphere−pentamers about 10%.

To estimate the contribution of particle heterogeneity to the width of the plasmon peak distributions (Figure 2a and b), we performed DDA simulations of plasmon coupling between the most likely contaminants (sphere−triangle and sphere−pentamer dimers). We held the particle volume fixed at the volume of an 80-nm sphere and the interparticle spacing to 19.1 nm and varied the shape. Compared to the peak plasmon of a sphere−sphere dimer, the peak plasmon of a sphere−triangular prism dimer was blue-shifted by 22 nm, and the peak plasmon of a sphere−pentagonal prism dimer was blue-shifted by 25 nm. The blue-shifting of the plasmon peak in these assemblies is expected because the coupling between two plasmons depends on the degree to which their normal modes overlap: any departure from an ideal sphere−sphere case will degrade coupling, blue-shifting the plasmon peak.

Concluding Remarks. Taken together, the experimental calibration experiments, the calculations, and the TEM
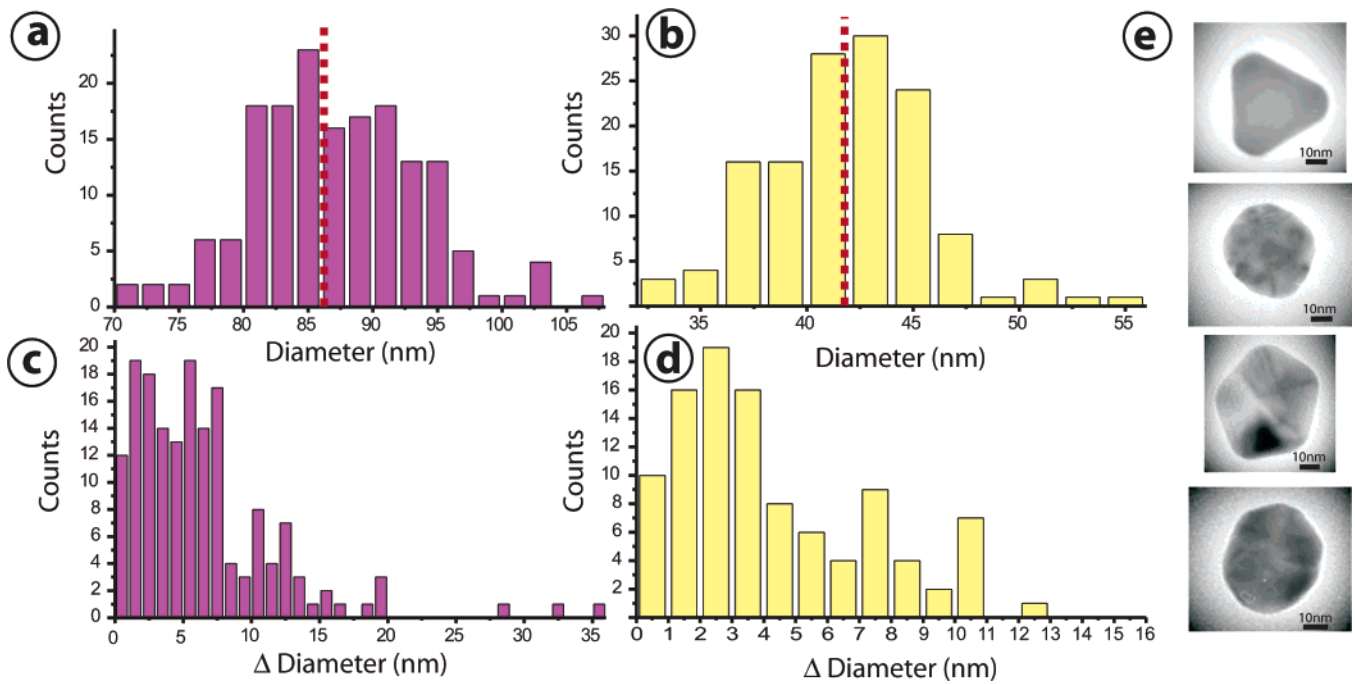
Figure 5. Heterogeneity of nanoparticle preparations. Size distributions for particles with nominal diameters of (a) 80 nm and (b) 40 nm obtained with transmission electron microscopy (TEM). Differences in diameter measured along two perpendicular axes for (c) 80-nm and (d) 40-nm Au nanoparticles. (e) TEM pictures of selected shapes found in the nanoparticle preparations.
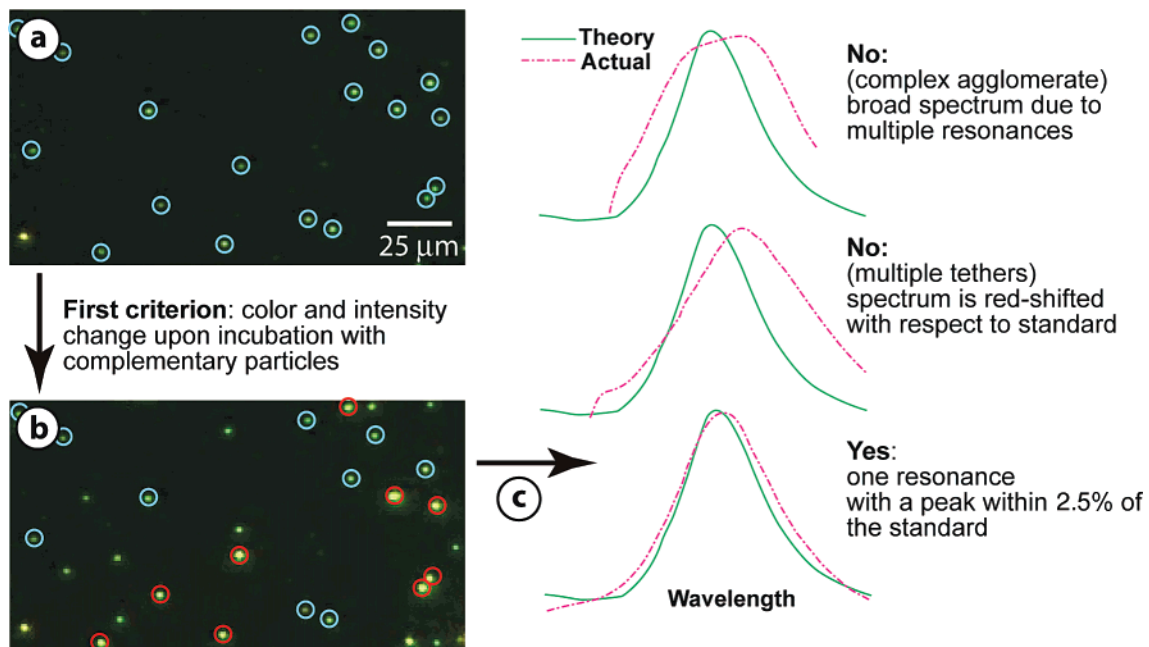

Figure 6. Improved procedure for use of plasmon rulers in single-molecule biophysics and nanotechnology. (a) First, a color CCD camera should be used to identify individual particles, as judged by their scattering intensity and color (blue circles). (b) Then, complementary particles should be introduced into the flow chamber, and scattering sources whose color and intensity changed should be located (red circles). (c) Finally, spectra for candidate plasmon rulers should be recorded, allowing identification of well-behaved plasmon rulers by comparison of its spectrum with a simulated or empirically obtained standard spectrum. All of these steps can be fully automated via suitable image processing software and a nanopositioning three-axis stage.

analyses of particle shapes reveal that plasmon rulers are already a useful material for single-molecule biophysics and nanotechnology. Even with a loose selection criterion for particle dimers and employment of heterogeneous off-the-shelf particle preparations, distances between 1 and 80 nm can be measured with a time resolution <50 ms (with 80-nm particles) and with absolute distance errors ranging from <1 nm to around 20 nm. Because of the steep slope of the λ_{PR} versus x relationship for 42-nm plasmon rulers, this ruler is most sensitive in the distance range between 0 and 20 nm; significantly larger distances can be measured with poorer spatial resolution. The λ_{PR} versus x relationship for

87-nm plasmon rulers is less steep, allowing the measurement of larger distances and distance changes, albeit with a reduced resolution. The accuracy of absolute distance measurements is limited principally by size and shape heterogeneity of the nanoparticles and the possibility of multiple tether formation between them.

The accuracy of plasmon rulers should improve more than 4-fold for the 42-nm particles and more than 10-fold for the 87-nm particles by employing a simple enrichment and validation procedure (Figure 6) that exploits a fundamental advantage of single-molecule approaches: ruler assembly can be monitored step by step, and at each stage, the nascent ruler can be compared to a predefined standard such as a simulated spectrum or empirically obtained standard spectrum. This procedure involves, per field of view, the acquisition of two color images, some simple image processing, and the subsequent acquisition of scattering spectra (Figure 6). Given our present setup and frame rates, and assuming the use of custom software and a commercial three-axis positioning system or a slitless spectrometer, we estimate that this procedure should identify $1-3$ well-behaved plasmon rulers per field of view per minute. This approach is conceptually identical to the one that has been refined over the past decade for single-molecule fluorescence experiments in which only FRET pairs fulfilling certain stringent criteria (e.g., anticorrelation of donor and acceptor emissions and single-step bleaching) are subject to further analysis.

To take full advantage of the long distance range of the plasmon ruler, synthetic strategies have to be developed to lower the surface density of tethering biopolymers and to improve the size and shape homogeneity of the nanoparticles. Both of these issues do not present fundamental limitations of the technique. Already, 10-nm gold nanoparticles can be functionalized routinely with a single DNA molecule,[37] and new promising synthetic approaches to better size and shape control, like the polymer-mediated polyol process, are being developed.[38]

Supporting Information Available: Materials and methods, determination of the DNA coverage of Neutravidin gold nanoparticle conjugates, and Figure S1. This material is available free of charge via the Internet at http://pubs.acs.org.

References

(1) Fennimore, A. M.; Yuzvinsky, T. D.; Han, W. Q.; Fuhrer, M. S.; Cumings, J.; Zettl, A. *Nature* **2003**, *424*, 408−410.

(2) Vale, R. D.; Milligan, R. A. *Science* **2000**, *288*, 88−95.

(3) Ha, T.; Enderle, T.; Ogletree, D. F.; Chemla, D. S.; Selvin, P. R.; Weiss, S. *Proc. Natl. Acad. Sci. U.S.A.* **1996**, *93*, 6264−6268.

(4) Ha, T. *Curr. Opin. Struct. Biol.* **2001**, *11*, 287−292.

(5) Ha, T. J. *Biochemistry* **2004**, *43*, 4055−4063.

(6) Weiss, S. *Science* **1999**, *283*, 1676−1683.

(7) Weiss, S. *Nat. Struct. Biol.* **2000**, *7*, 724−729.

(8) Yildiz, A.; Forkey, J. N.; McKinney, S. A.; Ha, T.; Goldman, Y. E.; Selvin, P. R. *Science* **2003**, *300*, 2061−2065.

(9) Zondervan, R.; Kulzer, F.; Orlinskii, S. B.; Orrit, M. *J. Phys. Chem. A* **2003**, *107*, 6770−6776.

(10) Lakowicz, J. R. *Principles of Fluorescence Spectroscopy*, 2nd ed.; Kluwer Academic/Plenum Publishers: New York, 1999.

(11) Wyman, C.; Rombel, I.; North, A. K.; Bustamante, C.; Kustu, S. *Science* **1997**, *275*, 1658−1661.

(12) Sonnichsen, C.; Reinhard, B. M.; Liphardt, J.; Alivisatos, A. P. *Nat. Biotech.* **2005**, *23*, 741−745.

(13) Kreibig, U.; Vollmer, M. *Optical Properties of Metal Clusters*; Springer: Berlin, 1995.

(14) Sonnichsen, C.; Geier, S.; Hecker, N. E.; von Plessen, G.; Feldmann, J.; Ditlbacher, H.; Lamprecht, B.; Krenn, J. R.; Aussenegg, F. R.; Chan, V. Z. H.; Spatz, J. P.; Moller, M. *Appl. Phys. Lett.* **2000**, *77*, 2949−2951.

(15) El-Sayed, M. A. *Acc. Chem. Res.* **2001**, *34*, 257−264.

(16) Kelly, K. L.; Coronado, E.; Zhao, L. L.; Schatz, G. C. *J. Phys. Chem. B* **2003**, *107*, 668−677.

(17) Yguerabide, J.; Yguerabide, E. E. *Anal. Biochem.* **1998**, *262*, 137−156.

(18) Mock, J. J.; Barbic, M.; Smith, D. R.; Schultz, D. A.; Schultz, S. *J. Chem. Phys.* **2002**, *116*, 6755−6759.

(19) Jin, R. C.; Cao, Y. W.; Mirkin, C. A.; Kelly, K. L.; Schatz, G. C.; Zheng, J. G. *Science* **2001**, *294*, 1901−1903.

(20) Mulvaney, P. *Langmuir* **1996**, *12*, 788−800.

(21) Haes, A. J.; Zou, S. L.; Schatz, G. C.; Van Duyne, R. P. *J. Phys. Chem. B* **2004**, *108*, 6961−6968.

(22) Raschke, G.; Kowarik, S.; Franzl, T.; Sonnichsen, C.; Klar, T. A.; Feldmann, J.; Nichtl, A.; Kurzinger, K. *Nano Lett.* **2003**, *3*, 935−938.

(23) McFarland, A. D.; Van Duyne, R. P. *Nano Lett.* **2003**, *3*, 1057−1062.

(24) Su, K. H.; Wei, Q. H.; Zhang, X.; Mock, J. J.; Smith, D. R.; Schultz, S. *Nano Lett.* **2003**, *3*, 1087−1090.

(25) Elghanian, R.; Storhoff, J. J.; Mucic, R. C.; Letsinger, R. L.; Mirkin, C. A. *Science* **1997**, *277*, 1078−1081.

(26) Maier, S. A.; Kik, P. G.; Atwater, H. A. *Appl. Phys. Lett.* **2002**, *81*, 1714−1716.

(27) Rechberger, W.; Hohenau, A.; Leitner, A.; Krenn, J. R.; Lamprecht, B.; Aussenegg, F. R. *Opt. Commun.* **2003**, *220*, 137−141.

(28) Haynes, C. L.; McFarland, A. D.; Zhao, L. L.; Van Duyne, R. P.; Schatz, G. C.; Gunnarsson, L.; Prikulis, J.; Kasemo, B.; Kall, M. *J. Phys. Chem. B* **2003**, *107*, 7337−7342.

(29) Wei, Q. H.; Su, K. H.; Durant, S.; Zhang, X. *Nano Lett.* **2004**, *4*, 1067−1071.

(30) Fromm, D. P.; Sundaramurthy, A.; Schuck, P. J.; Kino, G.; Moerner, W. E. *Nano Lett.* **2004**, *4*, 957−961.

(31) Kratky, O.; Porod, G. *Recl. Trav. Chim. Pays-Bas* **1949**, *68*, 1106−1122.

(32) Smith, S. B.; Cui, Y. J.; Bustamante, C. *Science* **1996**, *271*, 795−799.

(33) Draine, B. T.; Flatau, P. J. *J. Opt. Soc. Am. A* **1994**, *11*, 1491−1499.

(34) Mishchenko, M. I.; Travis, L. D.; Lacis, A. A. *Scattering, Absorption, and Emission of Light by Small Particles*; Cambridge University Press: Cambridge, 2002.

(35) Armstrong, S. H.; Budka, M. J. E.; Morrison, K. C.; Hasson, M. *J. Am. Chem. Soc.* **1947**, *69*, 1747−1753.

(36) Jung, L. S.; Campbell, C. T.; Chinowsky, T. M.; Mar, M. N.; Yee, S. S. *Langmuir* **1998**, *14*, 5636−5648.

(37) Zanchet, D.; Micheel, C. M.; Parak, W. J.; Gerion, D.; Alivisatos, A. P. *Nano Lett.* **2001**, *1*, 32−35.

(38) Wiley, B.; Sun, Y. G.; Mayers, B.; Xia, Y. N. *Chem.—Eur. J.* **2005**, *11*, 454−463.

NL051592S